BNL-105596-2014-TECH

BNL/SNS Technical Note No. 027;BNL-105596-2014-IR

Estimate of the Longitudinal Coupling Impedance for the NSNS Accumulator Ring

A. G. Ruggiero

April 1997

Collider Accelerator Department

Brookhaven National Laboratory

U.S. Department of Energy

USDOE Office of Science (SC)

DISCLAIMER

ESTIMATE of the LONGITUDINAL COUPLING IMPEDANCE for the NSNS ACCUMULATOR RING

BNL/NSNS TECHNICAL NOTE

NO. 027

A. G. Ruggiero and M. Blaskiewicz

April 21, 1997

ALTERNATING GRADIENT SYNCHROTRON DEPARTMENT
BROOKHAVEN NATIONAL LABORATORY
UPTON, NEW YORK 11973

Estimate of the Longitudinal Coupling Impedance for the NSNS Accumulator Ring*

A. G. Ruggiero and M. Blaskiewicz
Brookhaven National Laboratory

March 25, 1997

Introduction

The concept of longitudinal coupling impedance was introduced for the first time by Sessler and Vaccaro in 1967 [1] when the wall electromagnetic properties were approximated by a sequence of lumped components. It was subsequently re-examined in 1970-71 [2] in terms of the surface characteristic impedance. A similar concept was also adopted by Sacherer [3] in 1974. In this report we shall follow the concept expressed in these references. The definition relies on the smooth, homogeneous, and continuous properties of the vacuum chamber wall, as in the case of the resistivity of the wall. It was pointed out [2,4] that a beam of charged particles generates two types of electromagnetic fields that can act back on the beam. The two contributions add to each other. The first represents the electromagnetic field stored in the space between the beam and the vacuum chamber wall. It is independent of the wall properties, and primarily depends on the transverse dimensions of the beam and pipe. This contribution has an electric and a magnetic part which have tendency to cancel with each other, by exhibiting a γ^{-2} - dependence, where γ is the ratio of the total energy to the rest energy of a particle in the beam. This contribution is referred to as the "space-charge". The second contribution is proportional to the velocity βc of the beam, and it is otherwise independent of the beam energy. Nevertheless, this term depends very intimately on the electric properties of the vacuum chamber wall, and of the components located in its proximity. It represents the effect of the induced beam current flowing longitudinally along the wall and generating longitudinal fields as it encounters pipe resistivity and discontinuities.

The analytical estimate of the longitudinal coupling impedance relies on some model of the surrounding and on some approximation, for instance those relevant to the transverse geometry of the vacuum chamber and of the beam distribution. We shall follow below the circular geometry approximation [2,4], though other geometries have also been considered in the past: rectangular [4], elliptical [5], and axially displaced beam [6]. The theoretical model developed in [1-4] is essentially correct in the case of smooth vacuum chamber walls made of homogeneous and isotropic material. Moreover, it strictly applies only to the case the surface characteristic impedance is uniform and continuous along the wall, as in the case of the wall resistivity. The model also deals with a straight cylindrical pipe, whereas in reality the beam and the vacuum chamber are bent to form a toroidal shape. This may create a resonating behavior between the beam and the pipe which may be very important in high-energy storage rings [7]. Fortunately, this effect can be entirely ignored in the case of a relatively small storage ring and a sufficiently low-energy proton beam.

* Work performed under the auspices of the U.S. Department of Energy

All the other vacuum chamber components are really discontinuities of the vacuum pipe. They do not have then the smooth behavior of the resistivity of the wall. One can calculate wake fields left behind by the beam and average them out over the entire circumference. This approach, which is quite common and exploited, has been question in the past, for instance, in the case of striplines [8]. It seems that the actual distribution of identical devices around the ring may affect the frequency contain of the response triggered by the beam itself, which is the common source of fields to all the devices. Discontinuities of the vacuum chamber that are usually analytically estimated are: striplines for clearing electrodes and beam position monitors, vacuum chamber steps, bellows, vacuum ports, and RF cavities. A method was developed [7,9,10] to determine the longitudinal coupling impedance limit in a given particle accelerator, by gathering all the analytical equations available in the literature which provide the frequency dependence of the coupling impedance from different vacuum chamber components. This method is still in use these days. Alternatives are the use of numerical computer programs, like MAFIA [11] and ABCI [12], for more detailed evaluation, or measurement of the various vacuum components on a bench using the wire method. The beam itself, when it is available, may give information of the coupling to the surrounding by studying its behavior under controlled excitation.

A very important consideration is the nature of the vacuum chamber cutoff. Above a frequency which corresponds to a wavelength comparable or smaller than the vacuum chamber size, the longitudinal coupling impedance effectively vanishes [2,13], the beam is electromagnetically coupled to the free space, and the details of the vacuum chamber are no longer relevant. Even the free-space coupling impedance nevertheless has a cutoff-of its own. In the case of low-energy proton accelerators, the presence of the vacuum chamber wall completely screens the beam from the free-space and the beam is inhibited from radiating.

This technical note reports on the results of investigation of the longitudinal coupling impedance in the NSNS Accumulator Ring. Conventional formulae that can be found in the literature have been used, some of them with arguable validity. It is customary to define the ratio Z/n as the longitudinal coupling impedance where n is the harmonic number, the ratio of the frequency of interest to the revolution frequency.

The NSNS Accumulator Ring

The function of the Accumulator Ring is to take the 1.0 GeV proton beam from the Linac and convert the long Linac beam pulse of about 1 ms into a 0.5 second beam in about 1280 turns. The bunch compression occurs during the injection process, and the beam is immediately extracted at the end of the process. The final beam has an intensity of 2.08 x 10^{14} proton per pulse, resulting in 2 MW average beam power at 60 Hz repetition rate.

The lattice of the Accumulator Ring is a simple FODO lattice with four-fold symmetry [14], and the dispersion function is reduced to zero at straight sections by the missing magnet scheme. The total circumference of the ring is 220.7 m and the transition energy is $\gamma_T = 4.93$, higher than the operating energy of 1 GeV. The salient design parameters are shown in Table 1

Table 1: General Parameters of the NSNS Accumulator Ring

Average Power	2 MW
Kinetic Energy	1.0 GeV
Circumference, 2π R	220.7 m
Bending Field	7.4 kG
Number of Protons, N	2.08 x 10^{14}
Betatron Tunes, $Q_{H/V}$	5.8 / 5.8
Transition Energy, γ_T	4.93
Natural Chromaticity, $\xi_{H,V}$	-6.50, -7.29
Full Betatron Emittance, ε_{tot}	120 π mm mrad
Space-Charge Tune-Shift	< 0.2
RF peak Voltage (h=1)	42 kV
Revolution Frequency, f_0	1.1887 MHz
Filling Time	1.018 ms
Synchrotron Period, T_s	0.9 ms
Bunching Factor, B	0.325
Total Bunch Area, S	10 eV-s
Full Bunch Length, L	546.6 ns
Full Momentum Spread, Δ	1.6 %
Average Beam radius, a	3.80 cm
Average Pipe Radius, b	10 cm

The Ring Vacuum Pipe

The main parameters that enter the investigation are the dimension and the shape of the vacuum chamber, and the resistivity of the wall. The NSNS Accumulator Ring is made of three different sections: (i) The region of bending magnets where the shape of the vacuum pipe is rectangular with internal dimensions of 23 cm (H) and 13 cm (V). This region is expected to cover about 25 % of the whole ring circumference. (ii) The region of small quadrupoles where the vacuum pipe is circular with the internal diameter of 2b = 18 cm. This region is expected to cover about 60 % of the ring circumference. (iii) The region of large quadrupoles where also the pipe is circular but the internal diameter is 2b = 14 cm. This region covers the remaining 15 % of the circumference.

The analysis that follows applies strictly to circular geometry. Thus, we have approximated the rectangular vacuum chamber by a circular one with an internal diameter given by 2b = (H + V) / 2 = 18 cm. By taking an average of the pipe dimension around the ring we have then assumed a pipe with an internal radius b = 10 cm. For most of the chamber components entering the analysis, it is indeed sufficient to specify a single shape and a single dimension.

The material of the vacuum chamber can be either stainless steel with a surface resistivity of $\rho_w = 73\ \mu\Omega \times$ cm, or aluminum with $\rho_w = 2.83\ \mu\Omega \times$ cm. The vacuum system may require in some places stainless steel for more rigidity of the vacuum chamber and to avoid electron desorption at the wall. On the other end, the resistive wall instability may be softened by employing a higher conductor like aluminum.

Transverse Beam Dimension

The betatron emittance quoted in Table 1 defines the total beam, that is 100% of it. It has the same value in the two planes of oscillation. We adopted the criterion to define the total emittance ε_{tot} as 5 times the rms emittance ε_{rms}. We also define the average values of the envelope functions $<\beta_{H,V}> = R / Q_{H,V}$, with R the average closed orbit radius and $Q_{H,V}$ the betatron tunes. The average rms beam size in the vertical and horizontal plane are then given by $\sigma_{H,V} = (<\beta_{H,V}> \varepsilon_{rms})^{1/2}$. This is the contribution from the betatron motion alone, to which we should add the contribution in the horizontal plane from the relative momentum spread δ in the beam, which is $\sigma_E = <\eta> \delta$, where $<\eta> = R / \gamma_T^2$ is the average value of the dispersion around the ring. The total beam relative momentum spread Δ is given in Table 1. The rms value δ is 1/5 of the full value.

It is sometime required to specify the average beam radius around the ring. The assumption commonly made is that the beam has a transverse uniform charge distribution and a circular shape with radius a, which we estimate to be $a = 3 [\sigma_V (\sigma_H^2 + \sigma_E^2)^{1/2}]^{1/2}$.

Low-Energy Proton Storage Rings

The frequency range and the magnitude of the wall-coupling impedance in a storage ring is determined essentially by the dimensions of the vacuum chamber and by the energy of the beam through the relativistic factor γ, the ratio of the total beam energy to the rest energy. A major feature of a low-energy storage ring is the low value of γ and therefore of the impedance frequency range of interest. In fact the cut-off harmonic number above which the beam does not interact effectively with the wall components [2] is given by $n_c \sim \gamma R/b$, where R is the average ring radius and b is the average vacuum chamber size. For a 1 GeV proton energy, a circumference $2\pi R$ = 220.7 m and a vacuum chamber radius b = 10 cm, we derive $n_c \sim 726$, which is a very narrow frequency range (of only 0.61 GHz) when compared to that of high-energy storage rings (SSC, LHC, RHIC, Tevatron, ...).

Next we quote contributions to the longitudinal coupling impedance in the frequency range below the pipe cut-off. The actual numerical estimate over the entire frequency range will then include proper weighting due to the roll-off functions of the cut-off which are calculated as shown in Table 2.

Free-Space Impedance

Another major feature when compared to electron beams at ultra-relativistic velocities [9,10], is the complete screening of the beam from interacting with the free space and therefore the inhibition of radiation. In fact the cut-off for synchrotron radiation is $n_{rad} \sim 1.5\,\gamma^3$, considerably lower than the vacuum chamber cut-off n_c. In absence of the screening effect of a vacuum chamber, the free-space contribution to the longitudinal coupling impedance would otherwise be

$$Z/n \;=\; (177 \text{ ohm})\,(1.73 - i)\,n^{-2/3} \tag{1}$$

Table 3 gives the estimate of the residual free-space impedance for the NSNS Accumulator Ring which includes the cutoff screening functions shown already in Table 2.

The Curvature of the Vacuum Chamber

A particle circulating in a toroidal vacuum chamber is subject to resonances. A wave propagating at the outer side of the beam, though speeding at higher velocity, has nevertheless a longer trajectory than the beam which is moving to the inside at slightly less velocity. Therefore it is possible for the beam to catch up with the wave it radiated the revolution (or few revolutions) before. This is a condition for the "pipe resonances" [7]. For a circular pipe it can be written as

$$\beta\,(1 + b/R) \;=\; 1 \;+\; 0.80862\, n_r^{-2/3} \tag{2}$$

where n_r is the harmonic number value at resonance. It is immediately seen that one of the advantages of the low-energy storage ring is the absence of the vacuum chamber resonating modes that can be excited by the beam, because of the relative low value of the beam velocity β, and of the relatively large ratio of the pipe size b to the ring radius R.

Space-Charge Contribution

The space-charge contribution, that is the electromagnetic field stored in the region between the beam and the vacuum chamber, is [15]

$$Z/n \;=\; i\,Z_0\,(1 + 2 \ln b/a)\,/\,2\,\beta\gamma^2 \tag{3}$$

where $Z_0 = 377$ ohm, and $Z/n = 150i$ ohm, a purely "anti-inductive" contribution, which typically dominates over all other wall contributions in the case of a low-energy and relatively small proton storage ring.

The Space-Charge contribution to the NSNS Accumulator Ring is summarized in Table 4. Again, the roll-off due to the cutoff functions are also included.

Table 2: Cutoff Functions

Pipe Radius, b	10 cm	
Beam Size, a	37.9615743 mm	
a/b	0.37961574	
γ	2.06580266	
Radiation cutoff	13	10.9365323 MHz
Pipe cutoff	726	610.763268 MHz

n	Cut-Off Free-Space	Cut-Off Space-Charge	Cut-Off Pipe	nb/γR
1	0.99704579	0.99999986	0.99999905	0.00137741
2	0.98823543	0.99999945	0.99999621	0.00275482
3	0.97372416	0.99999877	0.99999146	0.00413223
4	0.95376566	0.99999781	0.99998482	0.00550964
5	0.92870467	0.99999658	0.99997628	0.00688705
6	0.89896707	0.99999508	0.99996585	0.00826446
7	0.86504789	0.9999933	0.99995352	0.00964187
8	0.82749757	0.99999125	0.99993929	0.01101928
9	0.78690719	0.99998893	0.99992316	0.01239669
10	0.74389306	0.99998633	0.99990514	0.0137741
20	0.30622598	0.99994532	0.99962062	0.02754821
30	0.06975809	0.99987697	0.9991466	0.04132231
40	0.00879363	0.9997813	0.99848334	0.05509642
50	0.00061343	0.9996583	0.99763124	0.06887052
60	2.368E-05	0.99950798	0.99659076	0.08264463
70	5.0584E-07	0.99933037	0.9953625	0.09641873
80	5.9796E-09	0.99912547	0.99394716	0.11019284
90	3.9116E-11	0.9988933	0.99234554	0.12396694
100	1.416E-13	0.99863388	0.99055855	0.13774105
200	4.0198E-52	0.99454671	0.96276571	0.27548209
300	2.288E-116	0.98777191	0.91816636	0.41322314
400	2.611E-206	0.97836464	0.85917662	0.55096419
500	0	0.9664011	0.78886707	0.68870523
600	0	0.95197749	0.71069869	0.82644628
700	0	0.93520869	0.62824278	0.96418733
800	0	0.91622679	0.5449163	1.10192837
900	0	0.89517929	0.46375906	1.23966942
1000	0	0.87222728	0.3872713	1.37741047

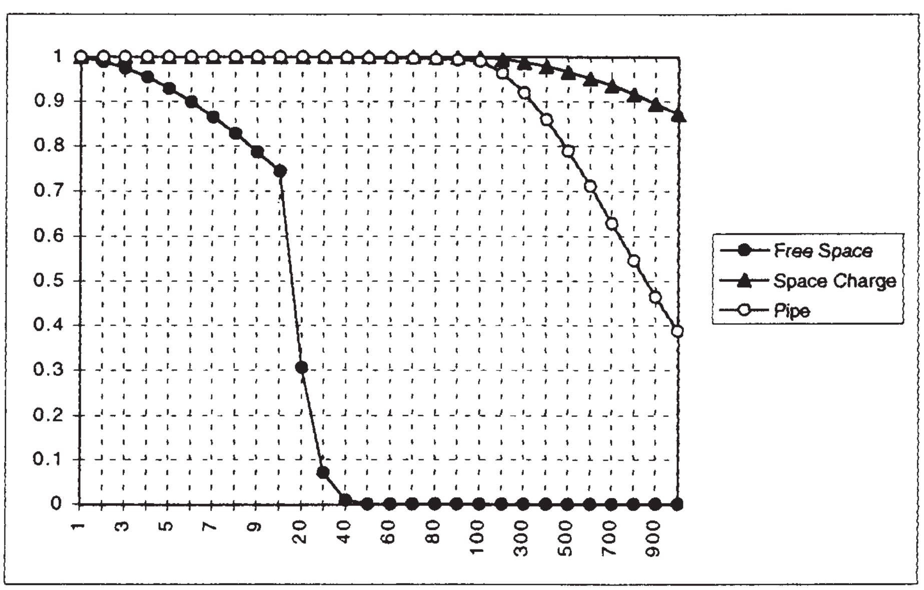

Table 3. Free-Space Residual Impedance (ohm)

Radiation cutoff	13 (n)	10.9365323 MHz	
Pipe cutoff	726 (n)	610.763268 MHz	

Full Screening

		Real	Imaginary	
Z/n	@ n = 726	none	none	ohm

n	Real	Imaginary
1	0.00028996	-0.0001674
2	0.00072421	-0.0004181
3	0.00122525	-0.0007074
4	0.00176123	-0.0010168
5	0.00230921	-0.0013332
6	0.00285038	-0.0016457
7	0.00336867	-0.0019449
8	0.00385039	-0.002223
9	0.00428411	-0.0024734
10	0.00466073	-0.0026909
20	0.00483389	-0.0027908
30	0.00189032	-0.0010914
40	0.00034958	-0.0002018
50	3.2823E-05	-1.895E-05
60	1.6149E-06	-9.323E-07
70	4.2342E-08	-2.445E-08
80	5.9764E-10	-3.45E-10
90	4.5706E-12	-2.639E-12
100	1.9023E-14	-1.098E-14
200	1.3417E-52	-7.746E-53
300	1.281E-116	-7.4E-117
400	2.076E-206	-1.2E-206
500	0	0
600	0	0
700	0	0
800	0	0
900	0	0
1000	0	0

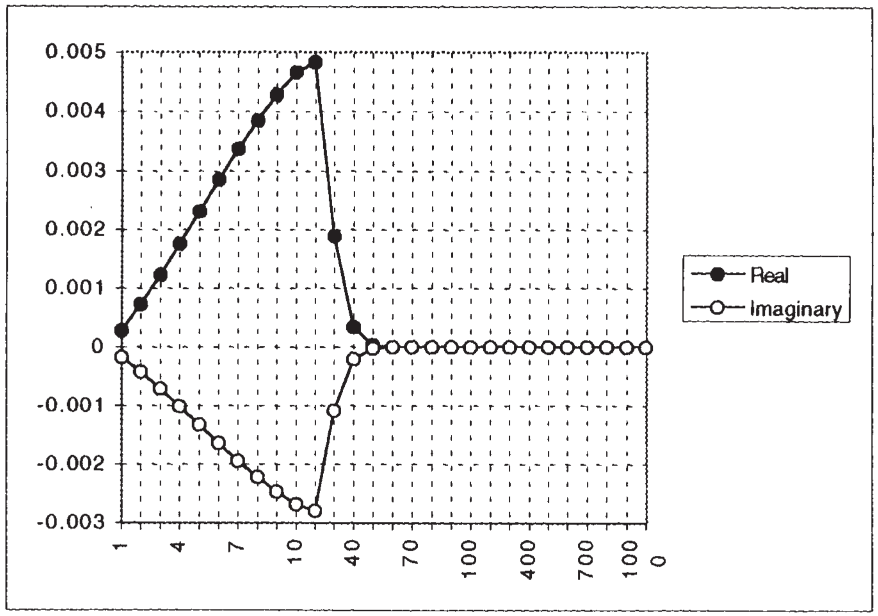

Table 4: Space-Charge Coupling Impedance (ohm)

Z/n 148.266927 ohm

n	Real	Imaginary
1	0	148.266907
2	0	148.266846
3	0	148.266744
4	0	148.266603
5	0	148.26642
6	0	148.266197
7	0	148.265934
8	0	148.26563
9	0	148.265285
10	0	148.2649
20	0	148.25882
30	0	148.248686
40	0	148.2345
50	0	148.216263
60	0	148.193977
70	0	148.167643
80	0	148.137263
90	0	148.10284
100	0	148.064377
200	0	147.458385
300	0	146.453905
400	0	145.059118
500	0	143.285321
600	0	141.146777
700	0	138.660519
800	0	135.84613
900	0	132.725483
1000	0	129.322458

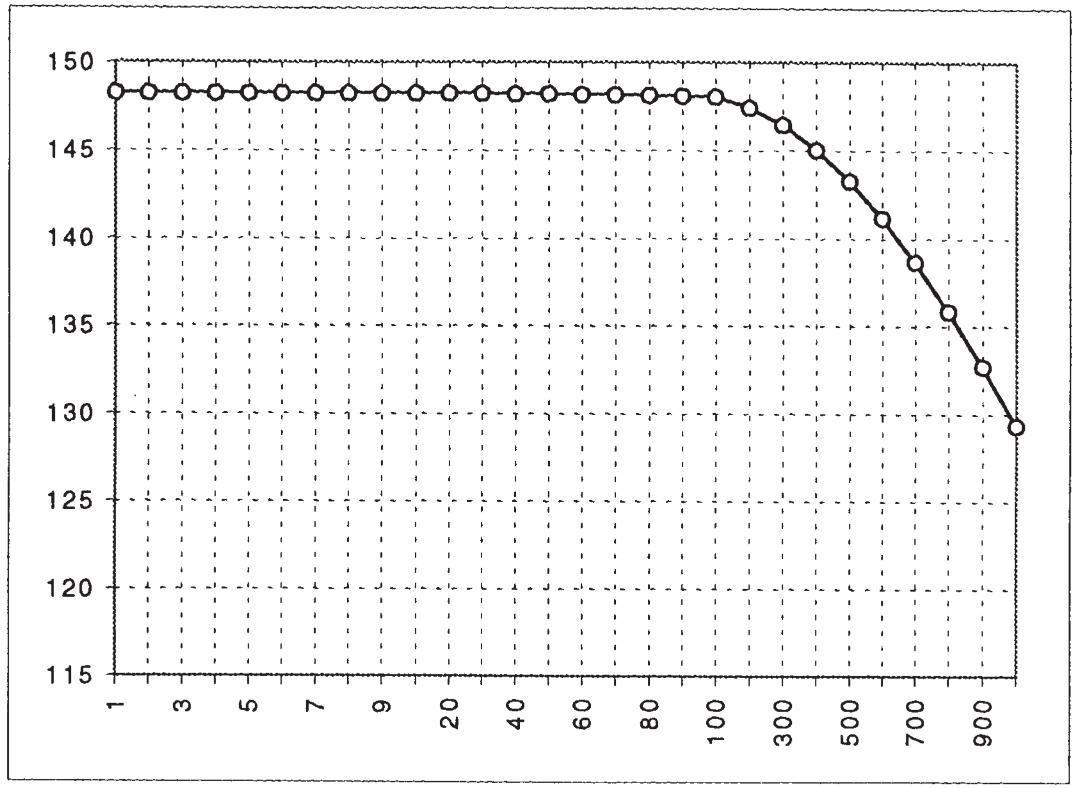

Table 5: Resistive-Wall Coupling Impedance (ohm)

Circumference	220.688 m			
Material	Stainless Steel	Copper	Aluminum	
Resistivity	73	1.8	2.83	μohm-cm
Fraction	**0.15**	**0**	**0.85**	
Skin Depth	0.38869706	0.061036	0.076532	mm @ n = 1

Average Wall Resistivity	3.687175	μohm-cm
Vacuum Chamber Thickness	**5**	mm
Pipe Radius	10	cm

Z/n @ n=1 0.15624351 -0.1562435 ohm $n^{-1/2}$

n	Real	Imaginary
1	0.15624336	-0.1562434
2	0.11048042	-0.1104804
3	0.09020646	-0.0902065
4	0.07812057	-0.0781206
5	0.06987256	-0.0698726
6	0.06378397	-0.063784
7	0.05905175	-0.0590517
8	0.05523707	-0.0552371
9	0.05207717	-0.0520772
10	0.04940385	-0.0494038
20	0.03492386	-0.0349239
30	0.02850169	-0.0285017
40	0.0246668	-0.0246668
50	0.02204383	-0.0220438
60	0.02010218	-0.0201022
70	0.01858807	-0.0185881
80	0.01736282	-0.0173628
90	0.01634345	-0.0163434
100	0.01547683	-0.0154768
200	0.01063672	-0.0106367
300	0.00828252	-0.0082825
400	0.00671204	-0.006712
500	0.00551215	-0.0055121
600	0.00453327	-0.0045333
700	0.00371006	-0.0037101
800	0.00301014	-0.0030101
900	0.00241531	-0.0024153
1000	0.00191345	-0.0019135

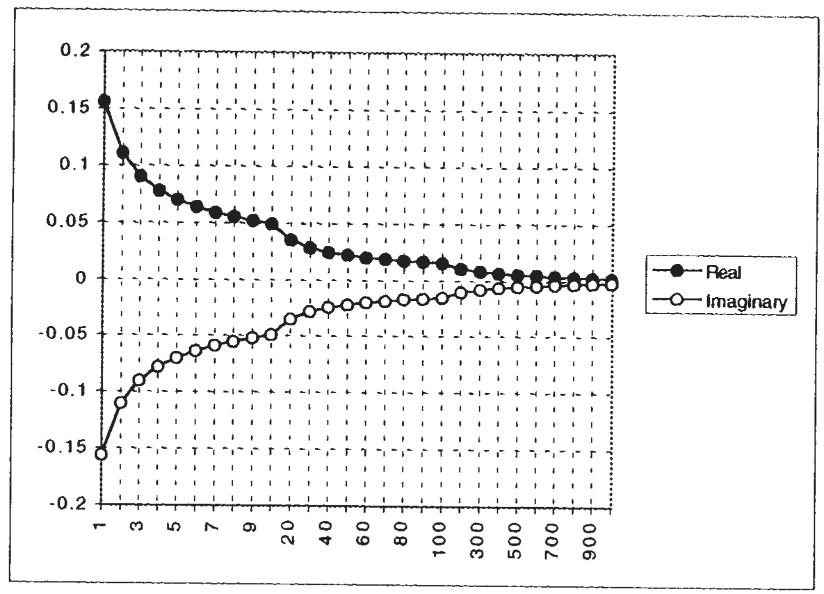

Resistivity of the Vacuum Chamber

The next contribution is the resistivity of the wall [4]

$$Z/n = (1 - i)(Z_0 \rho_w R / 2 b^2 n)^{-1/2} \tag{4}$$

The vacuum chamber is made 85% by Aluminum and 15% by Stainless Steel. For Aluminum $\rho_w = 2.83$ μohm-cm and for Stainless Steel $\rho_w = 73$ μohm-cm. The skin depth at the revolution frequency (n = 1) is 0.39 mm for Stainless Steel and only 0.08 mm for Aluminum. At the lowest harmonic n = 1, we have Z/n = (1 - i) 0.156 ohm as the total contribution of both types of vacuum chamber. The summary of the contribution from the resistivity of the wall is given in Table 5.

Vacuum Chamber Discontinuities

Next we have contributions which are caused by discontinuity of the vacuum chamber, like bellows, strip lines, vacuum chamber steps, vacuum pump ports, kicker magnets, and RF cavities. We shall examine them one-by-one below. The summaries of the details for each component are displayed in Tables 8 to 14.

Bellows:

Let M be the total number of bellows, m the number of convolutions per bellow, h the height and w the width of each convolution, then the contribution to Z/n in the low frequency range is [16]

$$Z/n = -i Z_0 (Mmw / 2\pi R) \ln(1 + h/b) \tag{5}$$

where $Z_0 = 377$ ohm. The values of the parameters are as shown in the Table 6 below.

Table 6. Bellows in the NSNS Accumulator Ring

Total Number, M	48
Number of Convolutions / Bellow	6
Height of Convolutions, h	25 mm
Width of Convolutions, w	10 mm
Pipe Diameter	20 cm
Lowest Resonating Frequency	3.0 GHz
Z/n @ n = 1	- 1.1 i ohm

Moreover, each convolution resembles a cavity resonating at frequencies $f_k = (1 + 2k)\, c/ 4h$ with

$k = 0, 1, 2, \ldots$. Fortunately, with the parameters of the NSNS Accumulator Ring, the lowest resonating mode is well above the vacuum-chamber cut-off so that the beam is not expected to be capable to excite these modes. The bellows are made of stainless steel, have a circular geometry and are a natural extension of the vacuum chamber, without any re-entrance attached that may look like a resonating object. Screening of the bellows with metallic fingers does not seem to be required.

Strip Lines:

They can be beam position monitors, clearing electrodes, transverse damper devices, and ferrite-loaded kickers for extraction. The last component deserves an analysis apart, given the complexity of the electrical configuration.

We shall assume M strip lines each made of m plates of width w. The characteristic impedance is Z_{cha}. The downstream end of each plate is shorted, whereas the upstream end is terminated to the characteristic impedance. The general expression of the contribution to Z/n is [13]

$$Z/n \;=\; -\,4i\, Z_{cha}\, (Mm\,/\,n)\, (w\,/\,2\pi b\,)^2 \exp(-i\,\omega\, d\,/\,c)\, \sin(\,\omega\, d\,/\,c\,) \tag{6}$$

where d is the length of a plate, and $\omega = n\,\beta c/R$. Strip lines do resonate at the harmonic number $n_{res} = c/(4d\, f_0)$, which is at about the vacuum chamber cut-off. There are 48 beam position monitors located next to each quadrupole magnet. Each station is made of 4 plates, 20 cm long and 7.5 cm wide. The characteristic impedance $Z_{cha} = 50$ ohm.

In the low frequency range $Z/n = -i\, 0.7$ ohm. The real part of the impedance peaks to about 0.5 ohm at the resonance. According to [8] the impedance given by Eq. (6) is to be multiplied by the following factor

$$\alpha_n \;=\; (1\,/M)\, \Sigma_s\, \exp(\,-\,i\, n\, z_s\,/\,R\,) \tag{7}$$

where z_s is the azimuthal location of the s-th plate around the circumference of the accelerator. For instance, in the case the position monitors have been distributed at equal distance, the factor α_n is always zero, except for those harmonics n which are multiple of the number M. This effect, which we believe applies as well to all other short discontinuous components, can be taken as an advantage when deciding how to place them around the ring.

Vacuum Chamber Steps:

The longitudinal coupling impedance of M single steps (uncoupled) was estimated by H. Hereward [17]

$$Z/n \;=\; 2\, M\, (\,1 - i\,\pi\,)\, Z_0\, (\,W - 1\,)^2\, b\,/\,2\,\pi^2\, R \tag{8}$$

for $n < n_W \;=\; 2\pi R\,/\,2b\,(\,W - 1\,)$, and for $n > n_W$

$$Z/n \;=\; Z_0\, M\,(\,W - 1\,)\,/\,2\pi n \tag{9}$$

where $W = b_2 / b_1$ is the ratio of the outer dimension b_2 to the inner dimension b_1 of the step.

According to this formula a substantial resistive contribution occurs in the low frequency range. It is associated to the actual energy loss suffered by a charged particle due to the diffraction phenomenon of an electro-magnetic plane wave being scattered by discontinuities. One should point out that very likely the result really applies only to wavelengths which have about the pipe dimension, that is in the proximity of the cut-off. Moreover, steps come in pair, an entrance followed by an exit discontinuity. Thus, one deals in reality with resonating cavities rather than single de-coupled steps. A step could be treated as a single discontinuity only at those wavelengths that are considerably shorter than the separation between the steps. The contribution represented by Eq.s (7 and 8) has been originally included in the analysis also for very low frequencies, but we believe that otherwise it should really not be included.

In any event, we have assumed 64 pairs of steps separated by about 2 m, with an inner radius of 10 cm and an outer radius of 13 cm. This yields $n_w = 3678$ (4.4 GHz), which is well above the pipe main cut-off, and $Z/n = (0.63 - 2.0\,i)$ ohm.

When this geometry was investigated numerically with ABCI it was not possible to derive any significant result. Only when the outer dimension was increased to about 20 cm, the program gave significant results with resonances which nevertheless appeared only at very large frequencies, in proximity of 0.6 GHz and above. The results are shown in Figures 1 and 2. A modest inductive contribution $Z/n = -i\,0.15$ ohm per cavity can be noticed in the low frequency range.

Vacuum Pump Ports:

These are circular openings of diameter d. The impedance is caused by the diffraction of the electro-magnetic wave through them. The impedance for M ports is [18]

$$Z/n = 2\,M\,Z_0\,\alpha^2\,[\,n^3 + i\,(8/\pi)\,(\,n^2\,n_{co} + n_{co}^3/3\,)\,]\,/\,3\,\pi^3\,R^4\,b^2 \tag{10}$$

where $n_{co} = 2\pi R / d$ and $\alpha = \pi\, d^3 / 16$.

We count 48 vacuum port with an opening of d = 10 cm. The resistive contribution to Z/n of the ports is negligible in the low-frequency range, and increases to a maximum of about 1/3 ohm above the pipe cutoff. Whereas there is a substantial contribution reactive of about 10 ohm (positive).

Damper System:

This is made of two parallel striplines [19] 2.5 meter long and 10 cm wide, loaded with ceramic having a relative dielectric constant $\varepsilon_r = 10$. The characteristic impedance of each line is $Z_{cha} = 50$ ohm. To allow for external powering, the plates are terminated at both ends to the characteristic impedance. The bandwidth is about 7 MHz centered to the resonating frequency of 10 MHz.

The impedance for such a device is [8,13]

$$Z/n = Z_{cha} (Mm / n) (w / 2\pi b)^2 [1 - \exp(i \omega d / c) \cos(\omega d / \beta c)] \qquad (11)$$

where M = 1 and m = 2, and the other notations are as defined for the similar Eq. (6). The estimate of the impedance is shown in Table 12. Most of the contribution, as it is expected. is in the low frequency range around the resonating frequency.

Kicker Magnets:

There are 8 magnets each of about 40 cm length. They are made of two copper coils of narrow rectangular shape surrounded by ferrite. They can also be treated as transmission lines in the way similar to the one used for strip lines in general. The complication nevertheless arises from the uncertainty to determine how the currents induced by the beam on the coils flow in and out of the system. The kicker magnets are to be activated only for a very brief period of time at the end of the accumulation process just to quickly extract the beam, in one turn, from the Accumulator Ring. Thus, since our concern is the interaction with the beam during the accumulation time, we shall assume that the magnets can be designed with the provision to allow shorting of each copper plate to ground at the down stream end, a short that will be opened with a fast switch at the moment of firing the magnets. Moreover, we shall assume that the characteristic impedance of each plate to ground is 50 ohm and that the geometry and properties of the ferrite will match this value. The upstream end will then be matched to the characteristic impedance. With this arrangement one can estimate the coupling impedance by utilizing Eq. (6). The results are given in Table 13. Most of the contribution, as expected, is in the low frequency range, where nonetheless especially the resistive contribution is substantial.

Clearly the kicker magnets deserves a closer and more detailed examination in the future, especially when the properties of the ferrite and the characteristic impedance of the plates have been determined more accurately. Also it is important to devise an electric arrangement which will allow indeed shorting of the downstream ends during the accumulation process of the beam.

RF Cavity System:

An RF cavity can always be approximated with an equivalent RLC parallel circuit, and be described by the resonating frequency, the figure of merit Q and the shunt impedance R_s. The RF Compression system is made of two subsets: the primary one working at the revolution frequency, and the second one tuned to the second harmonic. Main parameters are given in the Table 7 below.

Table 7. The Compression RF System of the NSNS Accumulator Ring

	System # 1	System # 2
Number of Gaps	6	2
Harmonic Number	1	2
Resonant Frequency	1.19 MHz	2.38 MHz
Q (unloaded)	200	200
Shunt Impedance	8 kohm	8 kohm

Table 8: Bellows Coupling Impedance (ohm)

Circumference	220.688 m		
Number of Bellows	**48**		
No. of Convolutions	**6**		
Height of Convolution	**25** mm		
Width of Convolution	**10** mm		
Pipe inner Radius	100 mm		
Pipe Cutoff	726 (n)	610.763268 MHz	
Z/n @ n=1	-1.097841 ohm		
Capacitance / unit length	2.78162897 pF/cm		
Inductance / unit length	707.499103 pH/cm		
Characteristic Impedance	15.9482614 ohm		
Resistivity	**73** μohm-cm	**stainless steel**	
Wall Impedance	14.7988229 ohm/cm		
Q	0.67712062		
Shunt Impedance	13.7495824 ohm/convolution		
Lowest resonating mode	2522 (n)	2997.925 MHz	
Z/n @ resonance	none	ohm	
relative freq. spread	**10** %		
Z/n with freq. spreading	none	ohm	

n	Real	Imaginary
1	0	-1.09784
2	0	-1.0978369
3	0	-1.0978317
4	0	-1.0978244
5	0	-1.097815
6	0	-1.0978035
7	0	-1.09779
8	0	-1.0977744
9	0	-1.0977567
10	0	-1.0977369
20	0	-1.0974245
30	0	-1.0969041
40	0	-1.096176
50	0	-1.0952405
60	0	-1.0940982
70	0	-1.0927498
80	0	-1.091196
90	0	-1.0894377
100	0	-1.0874758
200	0	-1.0569637
300	0	-1.0080007
400	0	-0.9432393
500	0	-0.8660506
600	0	-0.7802342
700	0	-0.6897107
800	0	-0.5982315
900	0	-0.5091337
1000	0	-0.4251623

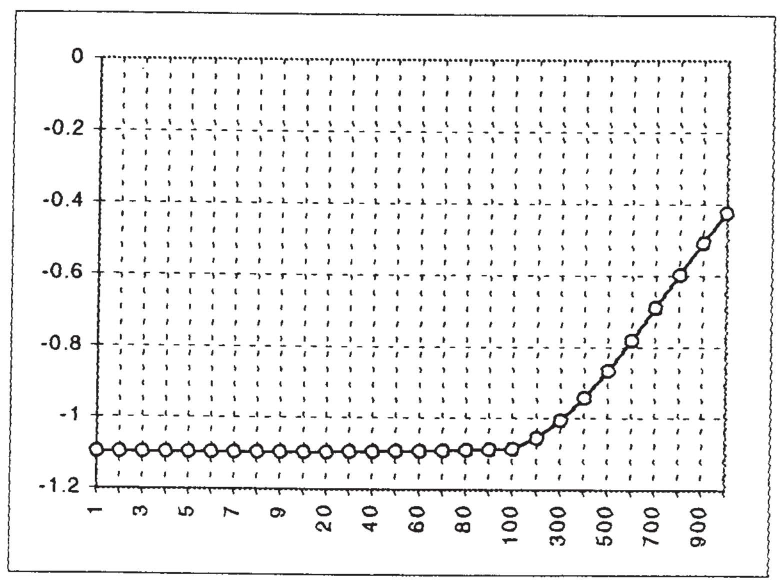

Table 9: Coupling Impedance from Beam Position Monitors (ohm)

Number	48	
No. of Plates	4	
Plate Length	20 cm	
Plate Width	7.5 cm	
Pipe Radius	10 cm	
Characteristic Impedance	50 ohm	
Z/n @ n=1	-0.6820926 ohm	
lowest resonating mode	315 (n)	374.740625 MHz
pipe cutoff	726 (n)	610.763268 MHz

n	Real	Imaginary
1	0.00340133	-0.6820807
2	0.00680247	-0.6820448
3	0.01020323	-0.681985
4	0.01360343	-0.6819014
5	0.01700288	-0.6817938
6	0.02040138	-0.6816623
7	0.02379875	-0.681507
8	0.0271948	-0.6813278
9	0.03058935	-0.6811247
10	0.0339822	-0.6808978
20	0.06777624	-0.6773215
30	0.10119542	-0.6713878
40	0.13405595	-0.6631366
50	0.16617834	-0.6526234
60	0.1973888	-0.6399188
70	0.22752055	-0.6251076
80	0.2564151	-0.6082885
90	0.2839234	-0.589573
100	0.30990698	-0.5690846
200	0.46463296	-0.3000918
300	0.41629577	-0.0311971
400	0.24410429	0.11014405
500	0.07867929	0.10387108
600	0.00359904	0.0238781
700	0.01436041	-0.0394549
800	0.05237728	-0.0462232
900	0.06699292	-0.0152907
1000	0.0490866	0.01381083

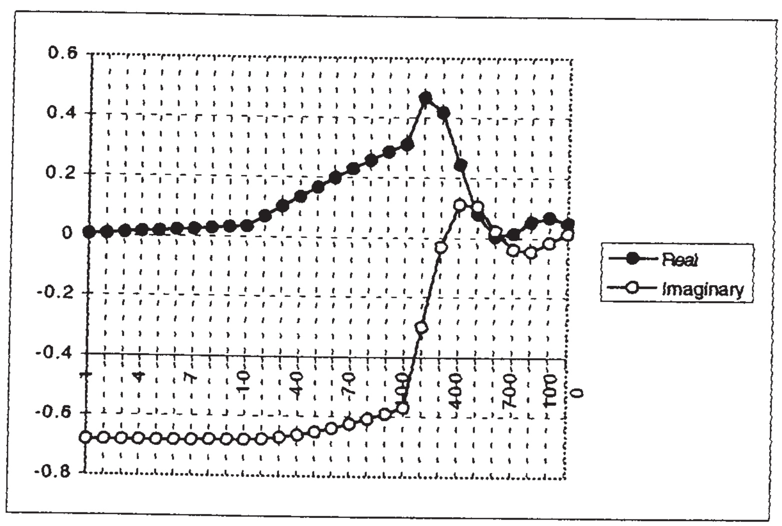

Table 10: Coupling Impedance of Vacuum Chamber Steps according to Hereward (ohm)

Number	**64**		
Pipe Radius inner	10 cm		
Pipe Radius outer	**13** cm		
Cutoff mode	3678 (n)		4371.95251 MHz
Z/n below cutoff	0.62641946	-1.96795476 ohm	
Z/n @ cutoff	0.00489408	0 ohm	
pipe cutoff	726 (n)		610.763268 MHz

n	Real	Imaginary
1	0.62641886	-1.96795289
2	0.62641708	-1.96794729
3	0.62641411	-1.96793796
4	0.62640995	-1.96792489
5	0.6264046	-1.96790809
6	0.62639806	-1.96788755
7	0.62639034	-1.96786329
8	0.62638143	-1.96783528
9	0.62637132	-1.96780355
10	0.62636003	-1.96776808
20	0.6261818	-1.96720816
30	0.62588487	-1.9662753
40	0.62546939	-1.96497005
50	0.62493562	-1.96329314
60	0.62428384	-1.96124552
70	0.62351444	-1.95882837
80	0.62262784	-1.95604305
90	0.62162456	-1.95289114
100	0.62050515	-1.94937442
200	0.60309517	-1.89467936
300	0.57515727	-1.80690986
400	0.53820495	-1.69082072
500	0.49416168	-1.55245471
600	0.44519548	-1.39862286
700	0.3935435	-1.23635336
800	0.34134617	-1.07237063
900	0.2905077	-0.91265684
1000	0.24259428	-0.7621324

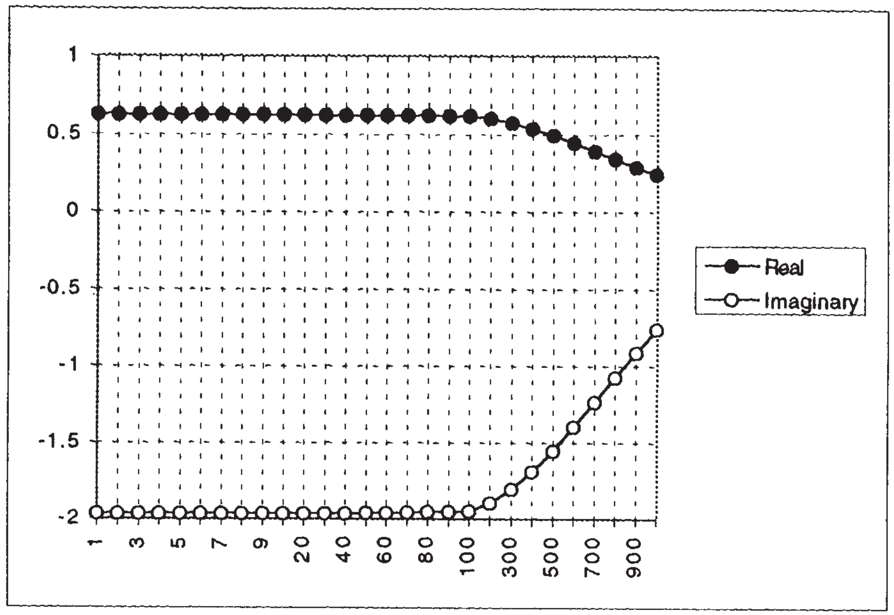

Table 11: Coupling Impedance of Vacuum Ports according to Sands (ohm)

Number	48	
diameter	10 cm	
alpha	196.349541 cm^3	
cutoff mode	2207 (n)	2623.40924
coherence	1	
Pipe Radius	10 cm	
Z/n @ n=1	9.8561E-10	8.99357198 ohm

n	Real	Imaginary
1	9.8561E-10	8.99356253
2	7.8849E-09	8.99355078
3	2.6611E-08	8.9935312
4	6.3078E-08	8.9935038
5	1.232E-07	8.99346855
6	2.1288E-07	8.99342548
7	3.3805E-07	8.99337458
8	5.046E-07	8.99331585
9	7.1845E-07	8.99324928
10	9.8551E-07	8.99317488
20	7.8816E-06	8.99200009
30	2.6586E-05	8.99004176
40	6.2973E-05	8.98729939
50	0.00012288	8.98377226
60	0.00021209	8.97945947
70	0.00033633	8.97435992
80	0.00050125	8.96847232
90	0.00071242	8.9617952
100	0.0009753	8.95432692
200	0.0075602	8.83566181
300	0.02420912	8.63517649
400	0.0533133	8.35024983
500	0.0947272	7.97972237
600	0.14581298	7.52562494
700	0.20196822	6.99451351
800	0.25749809	6.39807498
900	0.30663055	5.7528421
1000	0.34446129	5.07905822

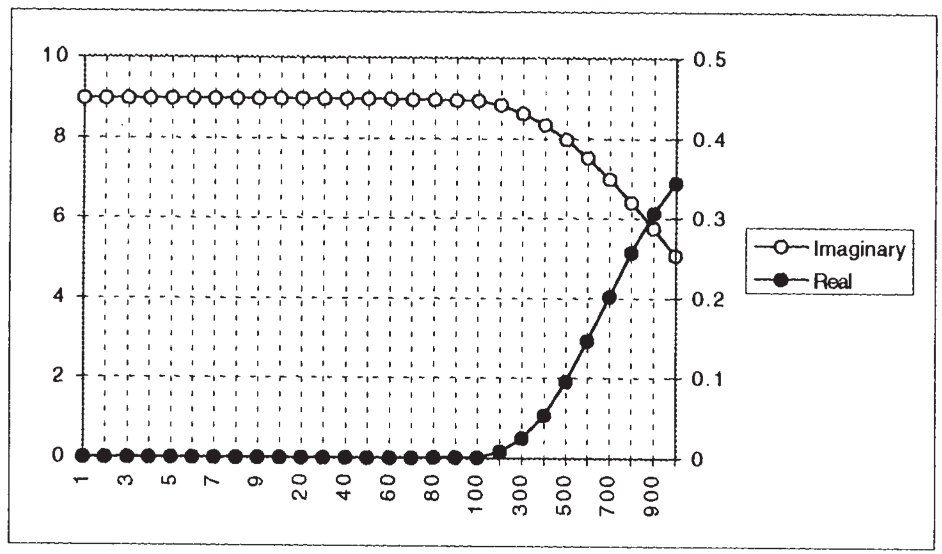

Table 12: Coupling Impedance (ohm) for the Damper System

Number of Systems	1	
Number of Plates	2	
Plate Length	250 cm	
Plate Width	10 cm	
Pipe radius, b	10 cm	
Permeability	1	
Dielectric	10	
Characteristic Impedance	50 ohm	
lowest resonating mode	8 (n)	9.48027125 MHz
pipe cutoff	726 (n)	610.763268 MHz

n	Real	Imaginary
1	0.11095551	-0.48178
2	0.21227678	-0.4366777
3	0.29545	-0.3667539
4	0.35405554	-0.2791922
5	0.38446906	-0.1827727
6	0.38620171	-0.0868042
7	0.36184107	-1.747E-05
8	0.31660948	0.07043487
9	0.2576075	0.11974423
10	0.19285211	0.14588326
20	0.1066706	-0.0199328
30	0.0141331	0.02908987
40	0.0632297	0.05696027
50	0.06091484	0.00429716
60	0.02351443	0.0185588
70	0.04980194	0.03327659
80	0.05107936	-1.201E-17
90	0.02554442	0.00575771
100	0.04108165	0.0159905
200	0.01219357	-0.007616
300	0.00652138	0.0012311
400	0.00424504	-5.874E-19
500	0.0057506	0.00175415
600	0.00300037	-0.0026977
700	0.00066587	0.00160749
800	0.00328405	1.5312E-18
900	0.00072524	-0.00058
1000	0.00098097	0.00022501

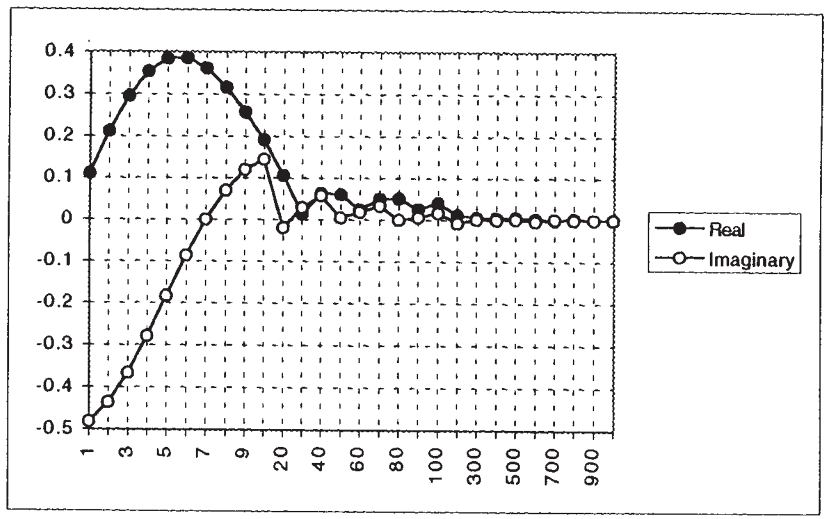

Table 13: Coupling Impedance (ohm) of the Kicker Magnets

Number of Systems	4
Number of Plates	2
Plate Length	40 cm
Plate Width	10 cm
Pipe radius, b	10 cm
Permeability	1000
Dielectric	1
Characteristic Impedance	50 ohm

lowest resonating mode	5 (n)	5.92516953 MHz
pipe cutoff	726 (n)	610.763268 MHz

n	Real	Imaginary
1	0.96753029	-2.977752
2	1.75027376	-2.4090452
3	2.21050032	-1.6060225
4	2.29111201	-0.7444274
5	2.02637562	-1.241E-16
6	1.52737903	0.49627553
7	0.94732133	0.68826923
8	0.43754353	0.60222701
9	0.10749521	0.33083623
10	1.5193E-32	1.2407E-16
20	3.0378E-32	1.2403E-16
30	4.5545E-32	1.2397E-16
40	6.0687E-32	1.2389E-16
50	7.5794E-32	1.2378E-16
60	9.0858E-32	1.2366E-16
70	1.0587E-31	1.235E-16
80	1.2082E-31	1.2333E-16
90	1.3571E-31	1.2313E-16
100	1.5051E-31	1.2291E-16
200	2.9258E-31	1.1946E-16
300	3.6031E-30	3.3426E-16
400	5.222E-31	1.0661E-16
500	1.2036E-29	4.3864E-16
600	5.5779E-30	2.5873E-16
700	2.2351E-30	1.4256E-16
800	6.6239E-31	6.7612E-17
900	8.0065E-32	2.0445E-17
1000	1.1817E-29	2.1534E-16

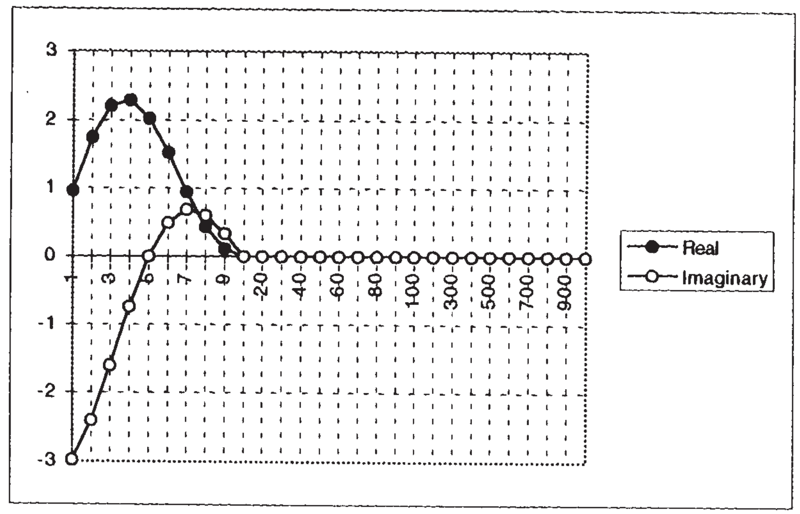

Table 14: Coupling Impedance (ohm) of the RF Cavity System

		System #1		System #2	
Number		6		2	
Harmonic Number		1		2	
Resonant Frequency		1.18867659 MHz		2.37735318 MHz	
Q		**2.00E+02**		**2.00E+02**	
Shunt Impedance		**0.008** Mohm		**0.008** Mohm	
Inductance		0.0053557 mH		0.00267785 mH	
Capacitance		3347.31381 pF		1673.65691 pF	
n		2		1	
omega	MHz	14.9373506		7.4686753	
denominator		9.0001		0.56250625	
Z/n @ n	ohm	0.2666637	79.9991111	0.1777758	-53.332741

n	Real	Imaginary
1	0.17777563	-53.33269
2	0.190681	79.9988076
3	0.23221334	61.9982133
4	0.05969773	29.3327115
5	0.02558846	17.6185757
6	0.01357733	11.8567153
7	0.00813748	8.55514662
8	0.00528479	6.47579103
9	0.00363513	5.07752812
10	0.00261136	4.09051861
20	0.00031174	1.00516254
30	9.1563E-05	0.44515447
40	3.8491E-05	0.24996474
50	1.9664E-05	0.15976164
60	1.136E-05	0.11080003
70	7.1418E-06	0.08129059
80	4.7763E-06	0.06214306
90	3.3485E-06	0.04901803
100	2.4363E-06	0.03963106
200	2.9586E-07	0.00962819
300	8.3595E-08	0.00408084
400	3.3E-08	0.00214797
500	1.5513E-08	0.0012622
600	8.0879E-09	0.00078967
700	4.5023E-09	0.00051285
800	2.6161E-09	0.00034057
900	1.5637E-09	0.00022902
1000	9.5195E-10	0.00015491

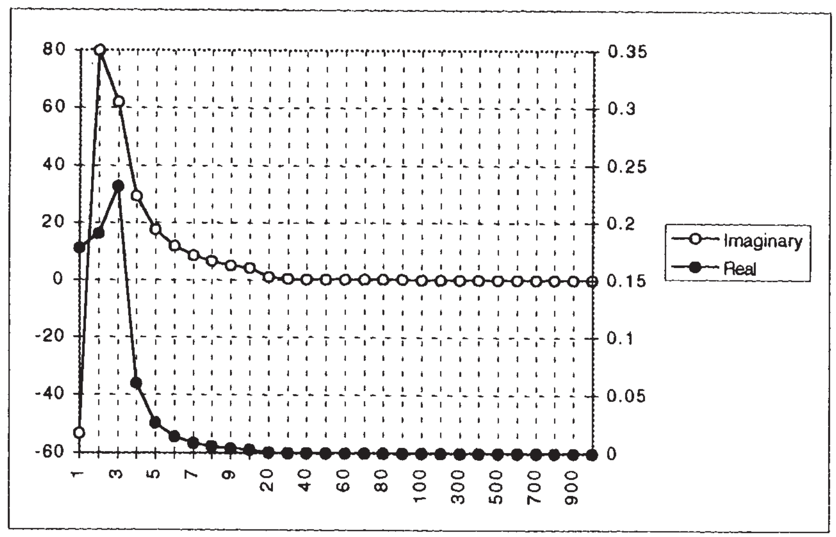

The RF system gives a large reactive contribution, second only to the space-charge term. Because of the relatively low figure of merit Q, there is also a substantial resistive contributions. In our analysis we have not included the impedance at the operating frequencies, since these are expected to be controlled and compensated with the low-level RF loops.

The Total Coupling Impedance of the NSNS Accumulator Ring

The total coupling impedance, that is the sum of all the contribution of the components presented above is given in Figure 1 versus the harmonic number n. The breakdown of the various contributions is shown in Tables 15 and 16. It is seen that at most the imaginary part is 230 ohm in the low-frequency range and about 150 ohm elsewhere. By far the largest contribution is the longitudinal space-charge, followed next by the RF cavity system. All other vacuum chamber components gave negligible imaginary contribution. On the other end, the resistive contribution at most is 3.5 ohm and always very small when compared to the imaginary term. In the large-frequency range, n > 10, the real part does not exceed 1 ohm. The kicker magnets are the major resistive source, followed, in the order, by the pipe steps, the damper system, and the resistivity of the wall with the RF cavity system.

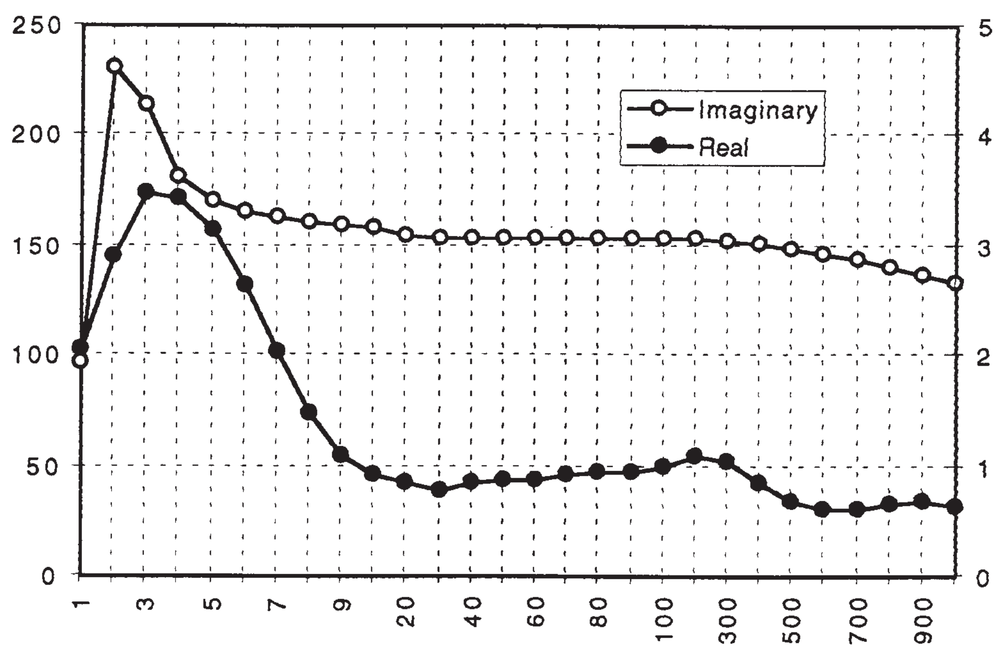

Figure 1. The Total Coupling Impedance in the NSNS Accumulator Ring

The analysis of which we have shown the results in this technical note does not include other special vacuum chamber items, specially those which are located in the injection region of the Accumulator Ring or other beam instrumentation devices.

Table 15: Coupling Impedance of the various contribution. Real Part (ohm)

Real n	Free Space	Space Charge	Resistive	Bellows	BPM	Damper	Kicker	Steps	Vaccum Ports	RF Cavities	Total
1	0.00028996	0	0.15624336	0	0.00340133	0.11095551	0.96753029	0.62641886	9.8561E-10	0.17777563	2.04261495
2	0.00072421	0	0.11048042	0	0.00680247	0.21227678	1.75027376	0.62641708	7.8849E-09	0.190681	2.89765573
3	0.00122525	0	0.09020646	0	0.01020323	0.29545	2.21050032	0.62641411	2.6611E-08	0.23221334	3.46621274
4	0.00176123	0	0.07812057	0	0.01360343	0.35405554	2.29111201	0.62640995	6.3078E-08	0.05969773	3.42476051
5	0.00230921	0	0.06987256	0	0.01700288	0.38446906	2.02637562	0.6264046	1.232E-07	0.02558846	3.15202251
6	0.00285038	0	0.06378397	0	0.02040138	0.38620171	1.52737903	0.62639806	2.1288E-07	0.01357733	2.64059206
7	0.00336867	0	0.05905175	0	0.02379875	0.36184107	0.94732133	0.62639034	3.3805E-07	0.00813748	2.02990972
8	0.00385039	0	0.05523707	0	0.0271948	0.31660948	0.43754353	0.62638143	5.046E-07	0.00528479	1.47210198
9	0.00428411	0	0.05207717	0	0.03058935	0.2576075	0.10749521	0.62637132	7.1845E-07	0.00363513	1.0820605
10	0.00466073	0	0.04940385	0	0.0339822	0.19285211	1.5193E-32	0.62636003	9.8551E-07	0.00261136	0.90987126
20	0.00483389	0	0.03492386	0	0.06777624	0.1066706	3.0378E-32	0.6261818	7.8816E-06	0.00031174	0.84070602
30	0.00189032	0	0.02850169	0	0.10119542	0.0141331	4.5545E-32	0.62588487	2.6586E-05	9.1563E-05	0.77172355
40	0.00034958	0	0.0246668	0	0.13405595	0.0632297	6.0687E-32	0.62546939	6.2973E-05	3.8491E-05	0.84787289
50	3.2823E-05	0	0.02204383	0	0.16617834	0.06091484	7.5794E-32	0.62493562	0.00012288	1.9664E-05	0.87424799
60	1.6149E-06	0	0.02010218	0	0.1973888	0.02351443	9.0858E-32	0.62428384	0.00021209	1.136E-05	0.86551431
70	4.2342E-08	0	0.01858807	0	0.22752055	0.04980194	1.0587E-31	0.62351444	0.00033633	7.1418E-06	0.9197685
80	5.9764E-10	0	0.01736282	0	0.2564151	0.05107936	1.2082E-31	0.62262784	0.00050125	4.7763E-06	0.94799114
90	4.5706E-12	0	0.01634345	0	0.2839234	0.02554442	1.3571E-31	0.62162456	0.00071242	3.3485E-06	0.94815159
100	1.9023E-14	0	0.01547683	0	0.30990698	0.04108165	1.5051E-31	0.62050515	0.0009753	2.4363E-06	0.98794835
200	1.3417E-52	0	0.01063672	0	0.46463296	0.01219357	2.9258E-31	0.60309517	0.0075602	2.9586E-07	1.09811892
300	1.281E-116	0	0.00828252	0	0.41629577	0.00652138	3.6031E-30	0.57515727	0.02420912	8.3595E-08	1.03046614
400	2.076E-206	0	0.00671204	0	0.24410429	0.00424504	5.222E-31	0.53820495	0.0533133	3.3E-08	0.84657964
500	0	0	0.00551215	0	0.07867929	0.0057506	1.2036E-29	0.49416168	0.0947272	1.5513E-08	0.67883092
600	0	0	0.00453327	0	0.00359904	0.00300037	5.5779E-30	0.44519548	0.14581298	8.0879E-09	0.60214116
700	0	0	0.00371006	0	0.01436041	0.00066587	2.2351E-30	0.3935435	0.20196822	4.5023E-09	0.61424806
800	0	0	0.00301014	0	0.05237728	0.00328405	6.6239E-31	0.34134617	0.25749809	2.6161E-09	0.65751574
900	0	0	0.00241531	0	0.06699292	0.00072524	8.0065E-32	0.2905077	0.30663055	1.5637E-09	0.66727172
1000	0	0	0.00191345	0	0.0490866	0.00098097	1.1817E-29	0.24259428	0.34446129	9.5195E-10	0.63903658

Table 16: Coupling Impedance of the various contribution. Imaginary Part (ohm)

Imagin.	n	Free Space	Space Charge	Resistive	Bellows	BPM	Damper	Kicker	Steps	Vaccum Ports	RF Cavities	Total
	1	-0.0001674	148.266907	-0.1562434	-1.09784	-0.6820807	-0.48178	-2.977752	-1.9679529	8.99356253	-53.33269	96.5639626
	2	-0.0004181	148.266846	-0.1104804	-1.0978369	-0.6820448	-0.4366777	-2.4090452	-1.9679473	8.99355078	79.9988076	230.554754
	3	-0.0007074	148.266744	-0.0902065	-1.0978317	-0.681985	-0.3667539	-1.6060225	-1.967938	8.9935312	61.9982133	213.447044
	4	-0.0010168	148.266603	-0.0781206	-1.0978244	-0.6819014	-0.2791922	-0.7444274	-1.9679249	8.9935038	29.3327115	181.74241
	5	-0.0013332	148.26642	-0.0698726	-1.097815	-0.6817938	-0.1827727	-1.241E-16	-1.9679081	8.99346855	17.6185757	170.876969
	6	-0.0016457	148.266197	-0.063784	-1.0978035	-0.6816623	-0.0868042	0.49627553	-1.9678876	8.99342548	11.8567153	165.713026
	7	-0.0019449	148.265934	-0.0590517	-1.09779	-0.681507	-1.747E-05	0.68826923	-1.9678633	8.99337458	8.55514662	162.69455
	8	-0.002223	148.26563	-0.0552371	-1.0977744	-0.6813278	0.07043487	0.60222701	-1.9678353	8.99331585	6.47579103	160.603001
	9	-0.0024734	148.265285	-0.0520772	-1.0977567	-0.6811247	0.11974423	0.33083623	-1.9678035	8.99324928	5.07752812	158.985407
	10	-0.0026909	148.2649	-0.0494038	-1.0977369	-0.6808978	0.14588326	1.2407E-16	-1.9677681	8.99317488	4.09051861	157.695979
	20	-0.0027908	148.25882	-0.0349239	-1.0974245	-0.6773215	-0.0199328	1.2403E-16	-1.9672082	8.99200009	1.00516254	154.45638
	30	-0.0010914	148.248686	-0.0285017	-1.0969041	-0.6713878	0.02908987	1.2397E-16	-1.9662753	8.99004176	0.44515447	153.948812
	40	-0.0002018	148.2345	-0.0246668	-1.096176	-0.6631366	0.05696027	1.2389E-16	-1.96497	8.98729939	0.24996474	153.779573
	50	-1.895E-05	148.216263	-0.0220438	-1.0952405	-0.6526234	0.00429716	1.2378E-16	-1.9632931	8.98377226	0.15976164	153.630875
	60	-9.323E-07	148.193977	-0.0201022	-1.0940982	-0.6399188	0.0185588	1.2366E-16	-1.9612455	8.97945947	0.11080003	153.58743
	70	-2.445E-08	148.167643	-0.0185881	-1.0927498	-0.6251076	0.03327659	1.235E-16	-1.9588284	8.97435992	0.08129059	153.561296
	80	-3.45E-10	148.137263	-0.0173628	-1.091196	-0.6082885	-1.201E-17	1.2333E-16	-1.956043	8.96847232	0.06214306	153.494988
	90	-2.639E-12	148.10284	-0.0163434	-1.0894377	-0.589573	0.00575771	1.2313E-16	-1.9528911	8.9617952	0.04901803	153.471166
	100	-1.098E-14	148.064377	-0.0154768	-1.0874758	-0.5690846	0.0159905	1.2291E-16	-1.9493744	8.95432692	0.03963106	153.452913
	200	-7.746E-53	147.458385	-0.0106367	-1.0569637	-0.3000918	-0.007616	1.1946E-16	-1.8946794	8.83566181	0.00962819	153.033687
	300	-7.4E-117	146.453905	-0.0082825	-1.0080007	-0.0311971	0.0012311	3.3426E-16	-1.8069099	8.63517649	0.00408084	152.240003
	400	-1.2E-206	145.059118	-0.006712	-0.9432393	0.11014405	-5.874E-19	1.0661E-16	-1.6908207	8.35024983	0.00214797	150.880888
	500	0	143.285321	-0.0055121	-0.8660506	0.10387108	0.00175415	4.3864E-16	-1.5524547	7.97972237	0.0012622	148.947914
	600	0	141.146777	-0.0045333	-0.7802342	0.0238781	-0.0026977	2.5873E-16	-1.3986229	7.52562494	0.00078967	146.510982
	700	0	138.660519	-0.0037101	-0.6897107	-0.0394549	0.00160749	1.4256E-16	-1.2363534	6.99451351	0.00051285	143.687924
	800	0	135.84613	-0.0030101	-0.5982315	-0.0462232	1.5312E-18	6.7612E-17	-1.0723706	6.39807498	0.00034057	140.52471
	900	0	132.725483	-0.0024153	-0.5091337	-0.0152907	-0.00058	2.0445E-17	-0.9126568	5.7528421	0.00022902	137.038478
	1000	0	129.322458	-0.0019135	-0.4251623	0.01381083	0.00022501	2.1534E-16	-0.7621324	5.07905822	0.00015491	133.226499

References

[1] A. Sessler and V.G. Vaccaro, Internal Yellow Report, CERN 67-2, Feb. 1967.
[2] A. G. Ruggiero, Fermilab Technical Notes FN-219, FN-220 and FN-230. (1970-71).
[3] F. Sacherer, Proc. of the 9th Int. Conf. on High Energy Accel., SLAC, 347, (May 1974).
[4] V.K. Neil and A.M. Sessler, Rev. Sci. Instr. 36, 429, (1965).
[5] A. G. Ruggiero, "Longitudinal Resistivity Wall Instabilities in an Intense Coasting Beam for Elliptic Geometry". ISR-SRM/67-13 (CERN, 1967).
[6] A. G. Ruggiero, "Longitudinal Resistivity Wall Instabilities in an Intense Coasting Beam for Axially Asymmetric Geometry". ISR-SRM/67-4 (CERN, 1967).
[7] A. Faltens and L.J. Laslett, Proc. of the 1975 ISABELLE Summer Study, vol. II, p. 486.
[8] A.G. Ruggiero and V.G. Vaccaro, "The Electro-Magnetic Field of an Intense Coasting Beam Perturbation in the Presence of Conductive Plates terminated at both Ends", Internal Report LNF -69/70, Frascati (Italy), Nov. 1969.
[9] A.G. Ruggiero, "Estimate of the Coupling Impedance for the Storage Rings of the NSLS", Informal Report BNL-27756, Brookhaven National Laboratory, August 1979.
[10] A.G. Ruggiero, "Some calculations for TRISTAN", KEK 80-16 (Japan), March 1981.
[11] T. Weiland, Particle Accelerators, Vol. 15 pp. 245-292 (1984).
[12] Yong Ho Chin, "User's Guide for ABCI, Version 8.7", CERN SL/94-02 (AP), Feb. 1994.
[13] A.G. Ruggiero, P. Strolin and V.G. Vaccaro, "Instabilities of an Intense Coasting Beam in the Presence of Conductive Plates", CERN ISR-RF-TH/69-7, March 1969.
[14] Y.Y. Lee, "The 4 Fold Symmetric Lattice for the NSNS Accumulator Ring", BNL/NSNS Technical Note No. 26, February 1997.
[15] C.E. Nielsen et al., Proc. of Int. Conf. on High Energy Accel., 239, CERN 1959.
[16] R. Briggs and V. Neil, Plasma Physics 8, 255 (1966).
[17] H.G. Hereward, CERN / ISR - DI / 75-47. (October 1975).
[18] M. Sands, Internal Report, PEP -253, September 1977.
[19] A.G. Ruggiero, "Fast Transverse damper for the NSNS Accumulator Ring", BNL/NSNS Technical Note No. 30, April 1997.